LA-UR-19-28220
Approved for public release; distribution is unlimited.

Title: Approach of a planar detonation to a steady CJ detonation wave

Author(s): Menikoff, Ralph

Intended for: Report

Issued: 2019-09-11 (rev.1)

Approach of a Planar Detonation to a Steady CJ Detonation Wave

Ralph Menikoff

September 9, 2019

Abstract

Generating a planar steady detonation wave in a high explosive is important for accurately measuring key parameters such as the CJ detonation state and the reaction-zone width. A detonation wave can be promptly shock initiated in the TATB based explosive PBX 9502 due to a fast hotspot reaction. However, a slow carbon clustering reaction causes the detonation wave to have a slow approach to steady state. Here we study the approach of the reaction zone of a planar detonation to the steady ZND profile of an underdriven detonation wave. For PBX 9502 simulations were run with the SURFplus reactive burn model. For comparison, simulations were also run with the HMX based PBX 9501. The SURF reactive model is used for PBX 9501 since it has only a fast hotspot reaction.

1 Introduction

A planar underdriven detonation wave is composed of a reaction zone triggered by a lead shock and followed by a rarefaction wave known as a Taylor wave. For a steady underdriven detonation wave, the reaction zone has a steady ZND profile and ends at a sonic point (CJ state) corresponding to the head of the rarefaction wave. The rarefaction wave spreads out with time but the head of the wave propagates with the steady detonation wave speed.

The TATB based explosive PBX 9502 has fast and slow reactions. The slow reaction makes it difficult to determine experimentally where the slow reaction ends and the Taylor wave begins. One approach tried to determine the CJ state by performing a series of experiments in which the detonation wave propagates for varying lengths of run at the end of which the velocity time history is measured with a PDV probe. By lining up the velocity profiles relative to the front, the end of the steady ZND profile should stand out from the non-steady release wave; see [Gustavsen et al., 2009, figs 1 & 2]. We show that this method for determining the CJ state only would work if the detonation waves have propagated sufficiently far for the reaction zone to have reached a steady state.

Here we study the approach of the reaction zone of a planar detonation to the steady ZND profile of an underdriven detonation wave using simulations with the SURFplus reactive burn model [Menikoff and Shaw, 2010, 2012] in the xRage code. The focus is on PBX 9502. But for comparison, simulations were also done for the HMX based explosive PBX 9501. This explosive has only a fast reaction and is expected to reach steady state much sooner.

2 PBX 9502 model

The simulations for PBX 9502 use the SURFplus reactive burn model [Menikoff and Shaw, 2012] with EOS and rate parameters specified in [Menikoff, 2017]. The model is composed of a fast hotspot reaction (SURF model) plus a slow reaction for the energy release as carbon clusters grow in size.

The rate for the hotspot reaction progress variable λ_1 is proportional to $(P/P_s)^n f(P_s)$ where P_s is the lead shock pressure and P is the local pressure. The SURF model includes a shock detector based on the Hugoniot energy function [Menikoff, 2016]. The shock detector determines both the shock pressure $P_s(x)$ and the shock arrival time $t(x)$. These quantities are useful for assessing the approach of a detonation wave to steady state.

The carbon clustering reaction is based on the diffusion limited cluster model of Shaw and Johnson [1987]. The SURFplus carbon cluster rate utilizes the steady detonation wave time

dependence for the reaction progress variable ($\lambda_2 = h(t)$) to build in the main properties of the diffusion model; the number of atoms in the cluster grows linear in time and the energy offset relative to equilibrium ($e_{cc}(t)$) is proportional to the surface-to-volume ratio of the cluster and hence decays as $t^{-1/3}$.

For ambient (room temperature and 1 bar) PBX 9502, the underdriven (CJ) detonation wave states from the EOS model are listed in table 1. The steady state carbon cluster reaction progress variable and energy offset are shown in fig. 1. We note that the carbon cluster energy release rate is proportional to $\mathsf{d}e_{cc}/\mathsf{d}t$. It starts out fast and then slows down significantly.

The approach of the detonation reaction zone to steady state undoubtably depends on the form of the carbon cluster rate as $\lambda_2 \to 1$. Since the model is physically based and calibrated to data, it should capture the main features of the approach to steady state and be semi-quantitative.

Table 1: Underdriven detonation wave states for ambient PBX 9502. CJ and VN denote Chapman-Jouguet and von Neumann, respectively.

	V cm^3/g	e MJ/kg	P GPa	T K	u_p km/s	c km/s	porosity per cent
Init state	0.52798	0.0	0.0001	300	0.0	1.944	2.5
detonation speed 7.782 km/s							
VN spike	0.32706	4.3850	43.65	1586	2.961	8.131	
CJ state	0.39808	1.8331	28.22	2955	1.915	5.867	

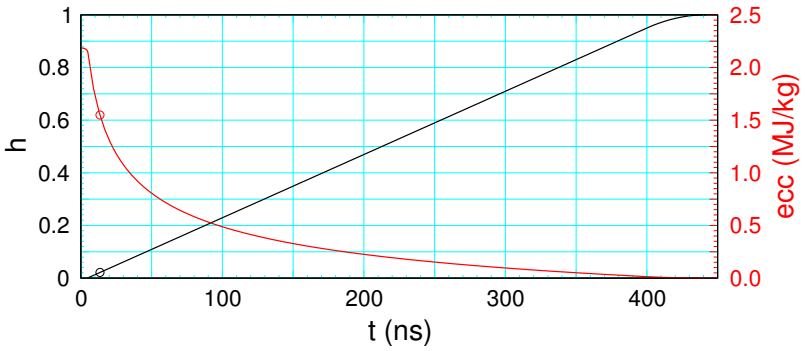

Figure 1: Steady state time dependence of $\lambda_2 = h(t)$ and carbon cluster energy offset $e_{cc}(t)$ relative to the equilibrium value. Open circles denote the values of λ_2 and e_{cc} at the end of the first reaction on the CJ detonation profile shown in fig. 3.

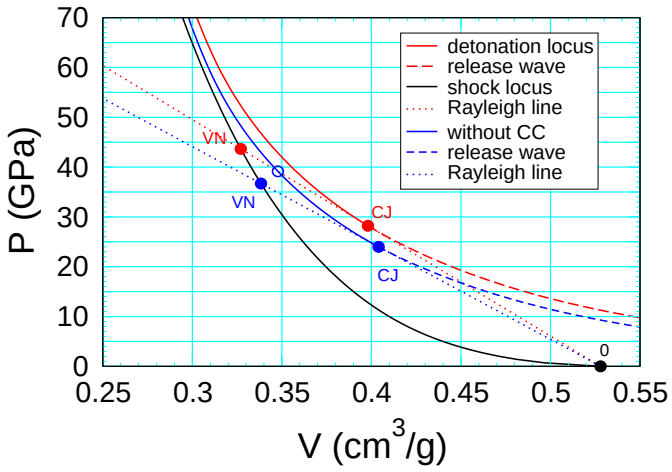

Figure 2: Shock locus and detonation loci with and without carbon clustering. Open blue circle denotes the pressure on the CJ Rayleigh line of the full reaction after the fast hotspot reaction has completed ($\lambda_1 = 1$).

The detonation loci with and without the carbon cluster energy is shown in fig. 2. Since the time scale for the fast reaction is substantially less than the time scale for the slow reaction, shock initiation is expected to transit to a detonation wave with detonation state approximately corresponding to the CJ state without the slow reaction. On a longer time scale, the energy released by the slow reaction would overdrive the fast reaction detonation wave leading to the detonation wave approaching the CJ state of the full reaction [Bdzil and Davis, 1975]. Since the end of the steady state reaction zone is sonic, the approach to steady state is expected to be much longer than the time scale for the slow reaction.

The steady ZND reaction-zone profile, shown in fig. 3, can be computed from ODEs using the explosive EOS and the reaction rates; see for example [Menikoff, 2015]). We note that at the end of fast reaction ($\lambda_1 = 1$) the pressure is 37.5 GPa, and the slow reaction progress variable is $\lambda_2 = 0.022$. From fig. 1, this corresponds to a carbon cluster energy (e_{cc}) release of 28 %; that is, there is significant clustering energy release towards the end of the fast reaction. The fast and slow reaction-zone widths are 0.120 and 2.530 mm. This corresponds to reaction times of 0.022 μs and 0.45 μs. The large disparity in widths and times is what leads to the slow approach of a detonation to steady state.

Finally, we note the depletion factor at end of both fast and slow reactions have been constructed to be proportional to $(1 - \lambda)^{1/2}$. This results in the pressure derivative at the end of reaction being finite and non-zero; see [Menikoff, 2015, pp 12-13].

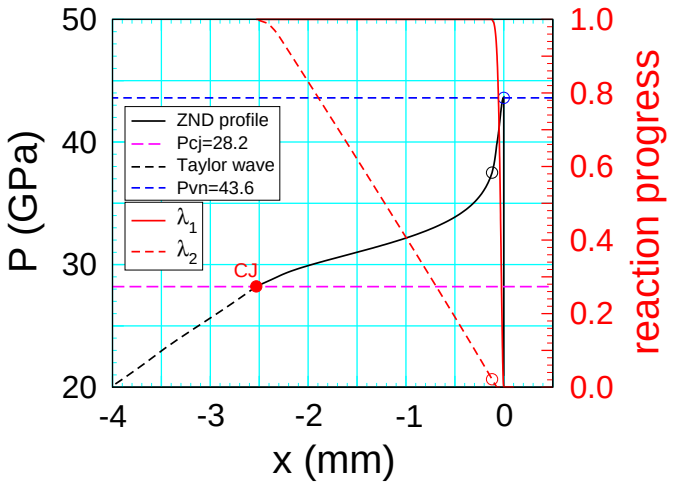

Figure 3: Steady state profiles for pressure and reaction progress variables. Solid red circle denotes the CJ state. Open black and red circles denote pressure and carbon cluster reaction progress variable, respectively, at the end of the hotspot reaction ($\lambda_1 = 1$).

3 Simulations

Simulations with the xRage code used a cell size of 4 μm to resolve the fast reaction and 32 μm for the slow reaction. A right facing detonation wave is promptly initiated with a 1 mm hotspot against a rigid wall on the left. The hotspot consisted of the products at the CJ state with a linear particle velocity from zero at the wall to the CJ particle velocity at the interface with the reactants. The detonation wave propagates out to 200 mm.

As a measure of the detonation wave approach to steady state, we use the dependence of the lead shock strength on distance of run. Both the VN spike pressure and the shock velocity can be determined from the lead shock detector of the SURF model. Short wavelength noise in the shock pressure is reduced by averaging over 4 cells. The shock speed is smoothed by using the slope of the shock trajectory $x(t)$ averaged over 2 mm (which is less than the CJ reaction-zone width).

3.1 Results for PBX 9502

The detonation wave speed and the lead shock pressure vs run distance show the approach to steady state; see fig. 4. Prompt initiation occurs within 5 mm of the hotspot, with the detonation wave having a speed and lead shock pressure below the CJ values by 2 % and 7.1 %, respectively.

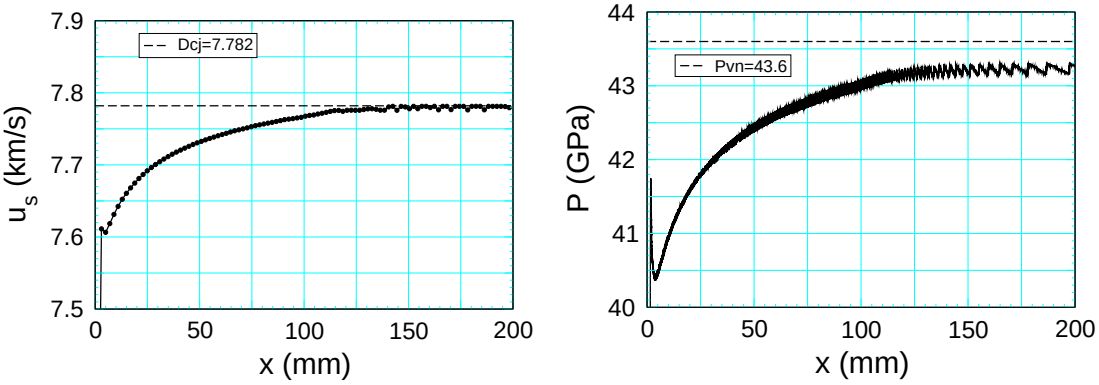

Figure 4: Detonation wave speed and lead shock pressure vs run distance for PBX 9502.

The pressure differs by a larger amount than the wave speed due to the tangency condition for the CJ state on the detonation locus in the (V, P)–plane; see fig. 2. After a run distance of about 150 mm, the detonation speed has nearly approached the CJ detonation speed, while the shock pressure levels off to a value below the VN spike pressure by about 1 %. The shock pressure also has a low amplitude ripple of about ± 0.2 %. Later we will see that the low shock pressure is due to a small amount of burning in the numerical shock profile, and the pressure ripple is due to the interpolation of the tabular EOS.

Plots of the pressure and reaction progress variable profiles at a sequence of time are shown in fig. 5. A key feature of the approach to steady state is that the value of the slow reaction progress variable at the CJ pressure increases with time; from 14 % at 1 μs to 57 % at 5 μs to the steady state value of 1 at 25 μs. We note that the fast reaction is fairly well resolved. However, zooming in on the lead shock shows that about 4 % burning in the shock rise; *i.e.*, $\lambda_1 \approx 0.04$

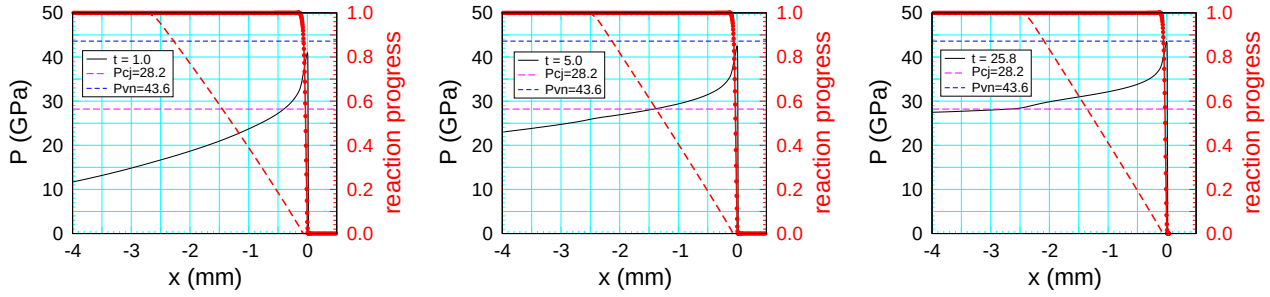

Figure 5: Profiles of pressure and reaction progress variables at a sequence of times. The solid and dashed red lines correspond to the fast and slow reactions, respectively. The red symbols denote the grid cells.

at the peak pressure corresponding to the lead shock. Compared with the semi-analytic ZND profile shown in fig. 3, the pressure profile at the end of the simulation is nearly the same. It differs slightly due to the low shock pressure which reduces the fast reaction rate by a small amount.

As a check on the simulated steady state detonation wave, profiles of the characteristic speed and pressure are shown in fig. 6. The plot shows that the sonic point (characteristic speed

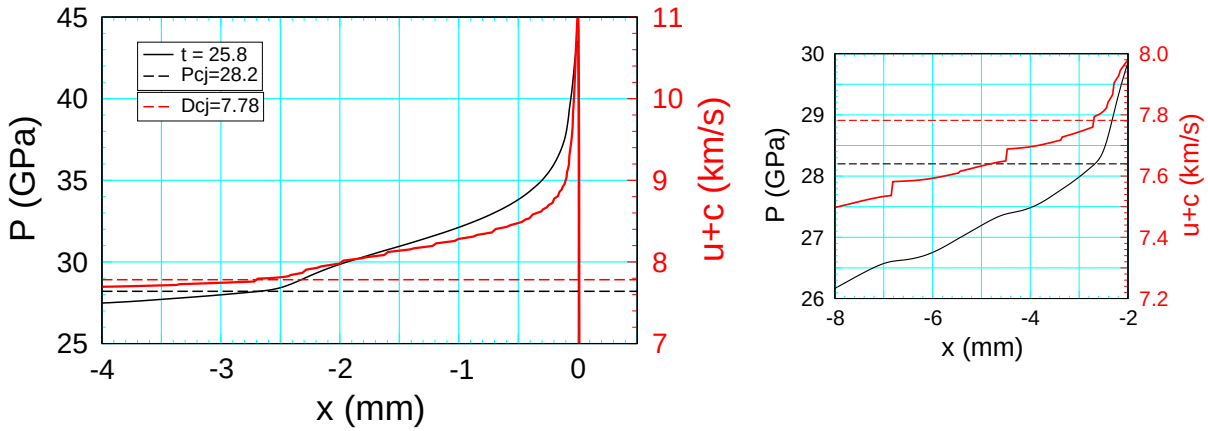

Figure 6: Characteristic speed and pressure profiles relative to shock front at end of simulation. Right plot is zoomed in on the head of the Taylor wave.

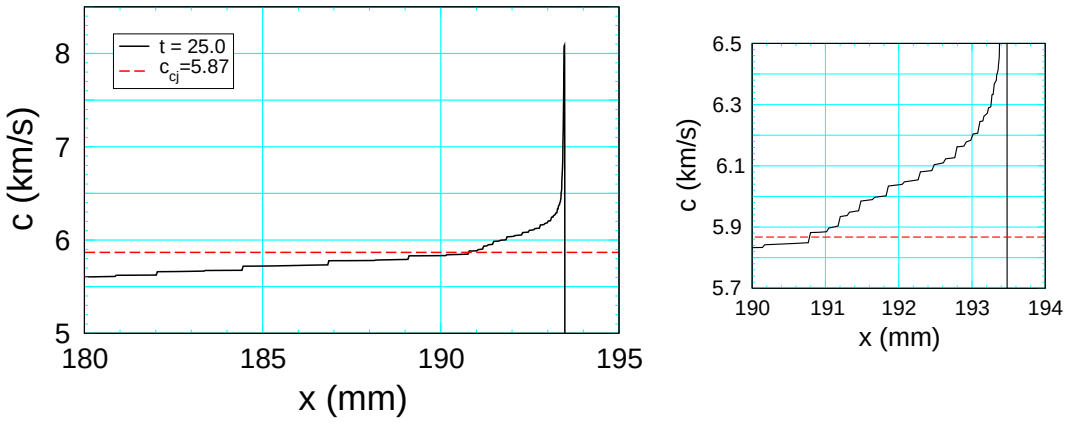

Figure 7: Profile of sound speed near end of simulation. Right plot is zoomed in on the slow rate portion of the reaction zone. Discontinuities are due to interpolation of the tabular EOS; normal derivatives along EOS grid lines are discontinuous.

crossing CJ detonation speed) corresponds to the pressure crossing P_{cj}. However, zooming in on the slow rate portion of the reaction zone and the head of the Taylor wave shows small jumps in the characteristic speed profile which gives rise to small amplitude undulation in the pressure profile.

Figure 7 shows that the jumps in the characteristic speed result from small discontinuities in the sound speed. The sound speed is expressed in terms of derivatives of the pressure, which depend on the interpolation of the tabular EOS. The xRage code interpolation is continuous for $\rho(P,T)$ and $e(P,T)$, but the derivatives normal to EOS grid lines have small discontinuities. Thus, the EOS interpolation results in jumps in the sound speed whenever the simulated profile in the (P,T) phase space crosses an EOS grid line. Since the Taylor wave is a right facing rarefaction, the pressure undulations spread out in time (*i.e.*, wave length increases) but do not dissipate.

The characteristic speed discontinuities within the slow rate portion of the reaction zone can be expected to generate acoustic noise. Since the reaction zone is subsonic, the noise will propagate into the fast rate portion of the reaction zone and introduce perturbations on the lead shock. This is the cause of the oscillations in the lead shock seen in fig. 4. As a check, a simulation was run with the slow reaction turned off. The result is similar to the simulation shown in the next section for PBX 9501 with the SURF model. Namely, the oscillations in the lead shock are greatly reduced.

A sequence of pressure profiles in the Lab frame are shown in fig. 8, and profiles shifted to have the origin at the shock front are shown in fig. 9. When the reaction zone is close to steady state, the CJ point can easily be picked out as the point at which the shifted profiles start to diverge. From fig. 9 this occurs after 11 μs which from fig. 8 corresponds to a run distance of about 70 mm.

Experimentally, propagating a detonation wave long enough to pick out the CJ state is problematic. Rarefactions from the side of the HE sample would lead to a curved detonation front and the sonic point would shift into the slow portion of the reaction zone. The sonic point, which is the analog of the planar CJ state, would have a lower pressure than the CJ pressure determined from the EOS.

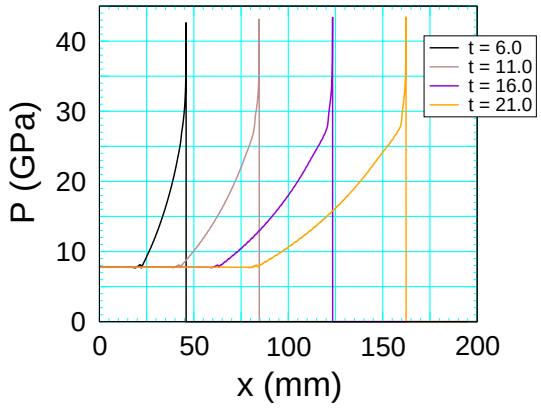

Figure 8: Sequence of pressure profiles for PBX 9502 in the Lab frame at selected times.

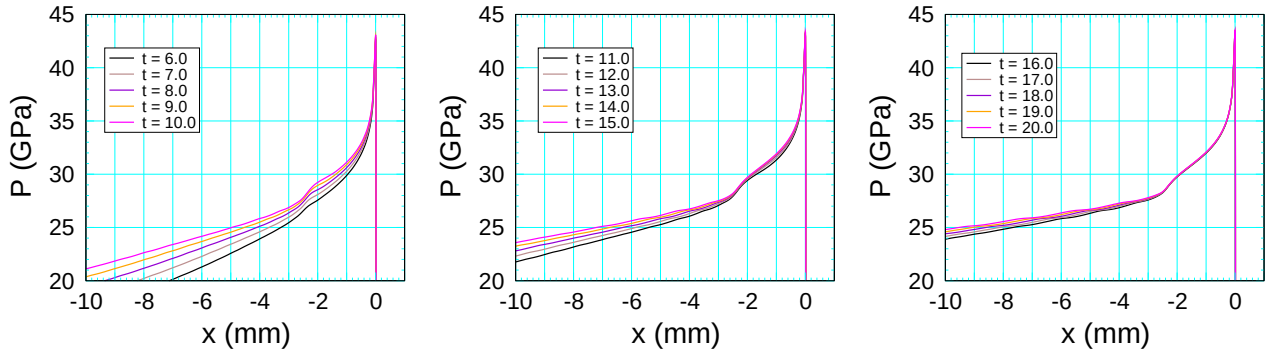

Figure 9: Pressure profiles for PBX 9502 relative to the front at sequence of times 1 μs apart.

3.1.1 Overdriven detonation

To see that the slow approach to the CJ detonation is largely due to the sonic point at the end of the reaction zone, a simulation was run with a slightly overdriven detonation wave. The simulation used a projectile instead of a hotspot to initiate and support a detonation wave. The projectile used the same EOS as the reactants and is given a velocity of 4.4 km/s. The initial shock match has a particle velocity of 2.2 km/s and shock pressure of 28 GPa. After the detonation wave is initiated, the projectile particle velocity drops to 2.07 km/s. This is slightly larger than the CJ particle velocity of 1.915 km/s. Therefore, the detonation wave is supported, and there is no Taylor wave.

Figure 10 compares the approach to a steady state for the supported and unsupported detonation. In both cases the VN spike pressure is slightly low due to a small amount of

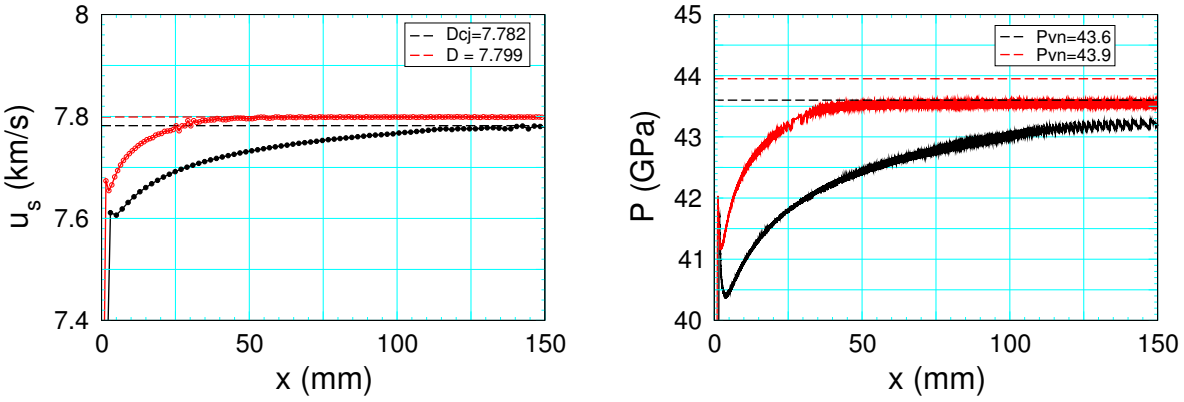

Figure 10: Comparison of detonation wave speed and lead shock pressure vs run distance for CJ detonation and slightly overdrive detonation in PBX 9502; black and red curves, respectively.

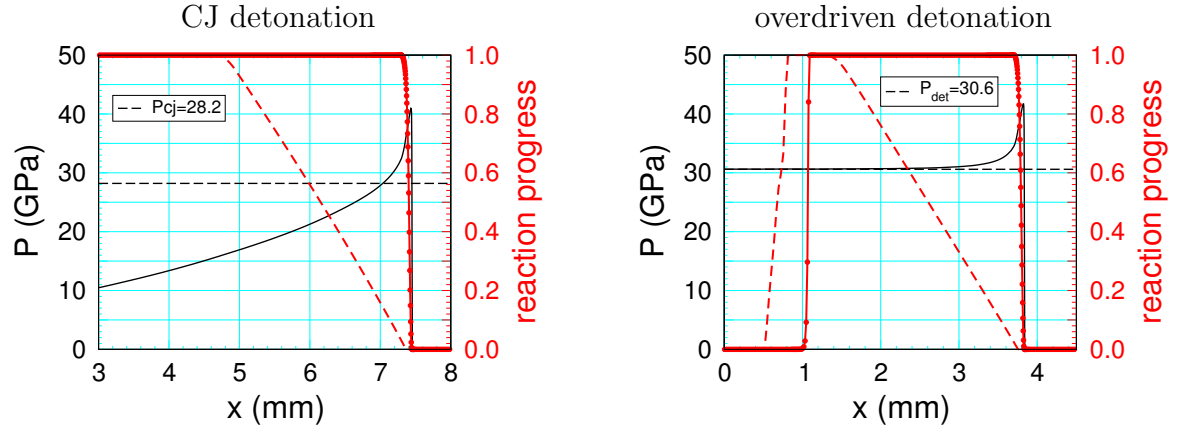

Figure 11: Comparison of pressure and reaction progress variable profiles for simulations at early time.

reaction in the shock profile. It can be seen that the overdriven detonation reaches steady state significantly faster than the CJ detonation.

A comparison of profiles at early times is shown in fig. 11. For the CJ detonation simulation, the pressure when the slow reaction completes is well below the CJ pressure due to the Taylor wave. In contrast, for the overdriven detonation, at the end of the reaction the pressure is within 0.6 % of the steady detonation pressure. This is largely due to the constraint imposed by the shock impedance match with the reacted products. However, just after ignition, fig. 12 shows that the reaction zone profile significantly differs from the steady state profile. One consequence, seen in fig. 10, is that the initial detonation speed is lower than the steady state value. In fact

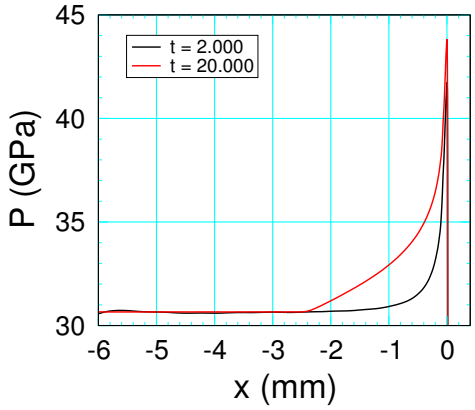

Figure 12: Comparison of pressure profiles at early and late times; *i.e.*, after ignition (black curve) and for steady state (red curve).

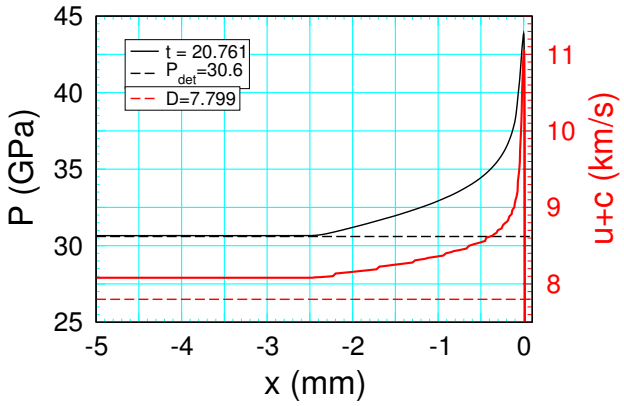

Figure 13: Characteristic speed and pressure profiles relative to shock front for overdriven PBX 9502 detonation wave.

it is less than D_{cj}. Another consequence is that the detonation pressure, determined from the jump condition $P = \rho_0 u_p D$ before steady state is reached, would also be lower than the steady state value. Even though the pressure profile looks like that of an overdriven detonation, if the profile is not steady, the detonation state is not on the overdriven detonation locus.

The characteristic speed for the CJ and overdriven cases are shown in fig. 6 and fig. 13, respectively. With respect to the front, the flow for the CJ detonation simulation is transonic, while the overdriven case is subsonic. A measure of the overdrive is $D/D_{cj} - 1 = 0.25\,\%$, and of of how subsonic the end of reaction zone is $(u + c)/D - 1 = 3.4\,\%$. For completeness, the ratio of the overdriven to CJ detonation pressure is $P_{overdriven}/P_{cj} - 1 = 8.5\,\%$.

3.2 PBX 9501

In contrast to the fast hotspot rate and slow carbon clustering rate of PBX 9502, the HMX based explosive PBX 9501 has only a fast hotspot rate. For comparison to PBX 9502, a simulation of the approach to steady state was run for PBX 9501 with the SURF model using rate parameters in table 2 and EOS given in [Menikoff, 2014].

In the detonation propagation regime, PBX 9501 has a faster hotspot rate than PBX 9502. A detonation wave is promptly initiated with a hotspot analogous to what was done for PBX 9502. The simulation also used the same 4 μm cell size to resolve the reaction zone.

The approach to steady state is shown in fig. 14. In contrast to PBX 9502 (fig. 4), the shock speed and lead shock pressure at the transition to detonation overshoot slightly. After 5 mm run, the steady state values are reached. We note that the numerical oscillations in the shock pressure seen for PBX 9502 is reduced to very low amplitude short wavelength noise which is eliminated by the smoothing previously described. A simulation for PBX 9502 without the slow reaction also does not show oscillations. This supports the claim that the oscillations for the

Table 2: SURF rate parameters for PBX 9501 for fitting form in [Menikoff, 2017, App. A].

		p_{scale}	1 GPa		
		t_{scale}	1 μs		
P_0	1.5	C	2.08e-2	s_1	2.0
P_{low}	3.5	f_n	2.35	P_{burn}	35.
P_1	45.	n	1.		
P_{hi}	60.	n_{hi}	0.		

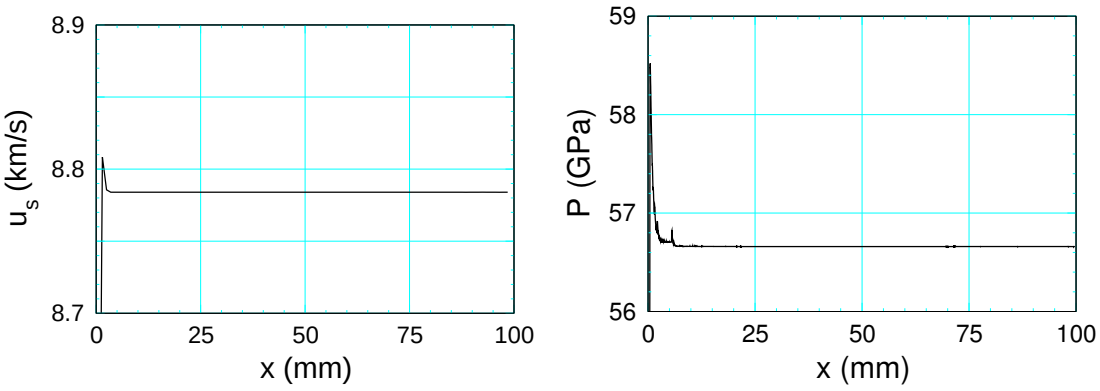

Figure 14: Detonation wave speed and shock pressure vs run distance for PBX 9501.

SURFplus PBX 9502 simulation is due to numerical noise generated in the slow reaction portion of the reaction zone.

Plots of the pressure and reaction progress variable (burn fraction of the products) at a sequence of times is shown in fig. 15. After 1 μs the reaction zone is steady. As a check, profiles of the characteristic speed and pressure are shown in fig. 16. The plot shows that the sonic point (characteristic speed crossing the CJ detonation speed) corresponds to the pressure crossing P_{cj}.

A time sequence of profiles relative to the front are shown in fig. 17. The CJ state corresponds to the point at which the Taylor waves start to diverge from the steady reaction zone. The slope of the pressure in the reaction zone due to the fast reaction is very large compared to the slope of the Taylor wave. Consequently, it is easy to pick out the CJ point, even for a single profile, from the kink in the pressure.

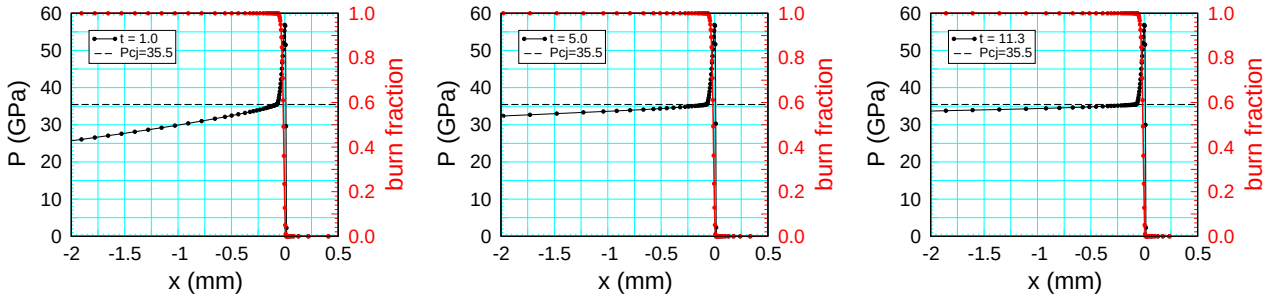

Figure 15: Profiles of pressure and reaction progress variable at a sequence of times.

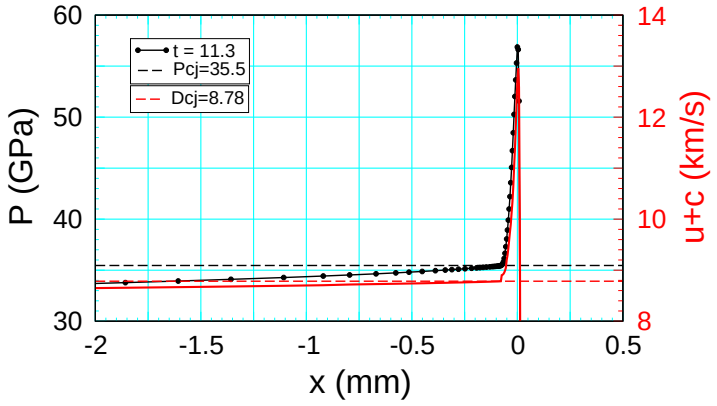

Figure 16: Characteristic speed and pressure profiles at the end of the simulation.

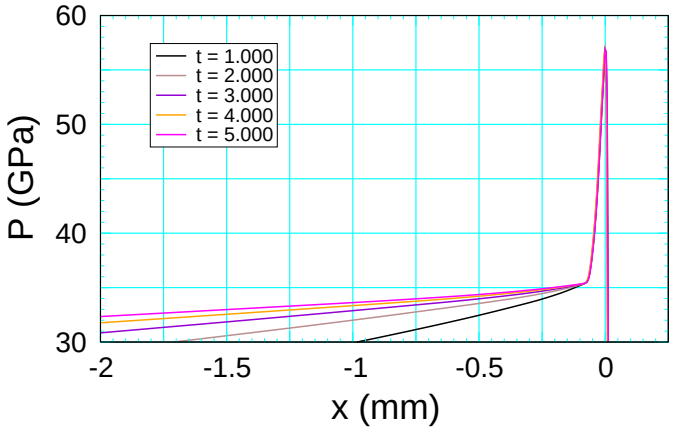

Figure 17: Pressure profiles for PBX 9501 relative to the front at sequence of times 1 μs apart.

3.3 Reaction zone profile experiment

Experiments to measure the CJ reaction zone profile have been done by placing a window at the end of the HE and using a VISAR or PDV probe to measure the particle velocity time history at the HE/window interface; see for example [Gustavsen et al., 1998]. In contrast to a PBX with a fast and slow reaction rates, experiments for a PBX with only a fast reaction rate do not suffer from the need to maintain a planar detonation for a long distance of run in order for the reaction zone to reach steady state.

The impedance mismatch when the detonation wave impacts the window is usually accounted for utilizing the graphical solution shown in fig. 18. It is assumed that CJ detonation speed has been previously measured. Hence, the slope of the Rayleigh line ($\rho_0 D_{cj}$) is known. In contrast to EOS measurements, the graphical solution for P_{vn} and P_{cj} is only approximate.

The issue with determining P_{vn} is that the reflected wave is in the HE sample and not the window material for which the EOS is known. The $P(u)$ curve, for both a shock and rarefaction, to second order can be expressed as

$$P(\Delta u) = \rho_{vn}\,\Delta u\,(c_{vn} + \tfrac{1}{2}\mathcal{G}_{vn}\Delta u) + \mathcal{O}\big((\Delta u)^3\big) \tag{1}$$

where the fundamental derivative $\mathcal{G} = \frac{1}{2}(V^3/c^2)(\partial^2 P/\partial V^2)_s$ characterizes the curvature of an isentrope. The density at the VN state is determined by P_{vn}, D_{cj} and the shock jump conditions. However, c_{vn} is not a priori known. Experiments with two different window leads to 2 equation for P_{vn} and c_{vn} which would enables P_{vn} to be determined to first order in Δu.

The issue with determining P_{cj} is that the pressure decreasing wave in the window material from the match to the VN state to the match to the CJ state is not a simple rarefaction

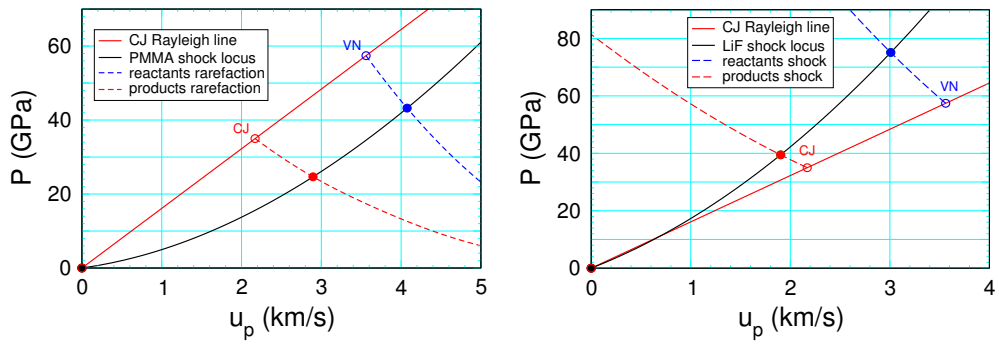

Figure 18: Approximate graphical solution to impedance match for a PBX 9501 detonation wave impacting a window. The left and right plots are for low (PMMA) and high (LiF) impedance windows, respectively.

(entropy and one Riemann invariant constant) for which the $P(u)$ curve is independent of the flow. Though it is likely using $P(u)$ for a rarefaction would be good to a couple of per cent since for a stiff window material the thermal component of the pressure is small compared to the compressive or density component.

The velocity data from a reaction zone experiment is better suited to use as validation test on a calibrated reactive burn model than as a means for accurately measuring the CJ pressure. A variation of this type of experiment may be better able to determine the CJ pressure at the expense of information on the reaction zone.

For a conventional explosive (HE with a narrow reaction zone), an old technique for determining the CJ pressure is with a series of experiments in which a detonation wave drives metal plates of various thicknesses. The free surface velocity of the plate is measured and then extrapolated to zero thickness. The extrapolated free surface velocity and the metal EOS determines the shock pressure corresponding to the CJ state; see [Duff and Houston, 1955] and analysis in [Bdzil and Davis, 1975].

The idea is that the high pressure in the reaction zone decays very rapidly when a detonation wave impacts an inert. In effect, the detonation wave can be approximated as a discontinuity to the CJ state. The match into the inert is a shock to the CJ pressure which then decays reflecting the Taylor wave behind the detonation. The extrapolation with plate thickness is to CJ pressure at the head of the Taylor wave.

Instead of measuring the free surface velocity of a plate, a split window with a thin aluminum reflector at the internal interface can be used with a PDV probes to measure the particle velocity at various distances of shock propagation in the window. Then extrapolate as before to the

particle velocity corresponding to the shock match from the CJ detonation state in the products to the window. This avoids the issue with a non-simple wave in the window. Furthermore, the slope of the release wave from the CJ products state can be expressed in terms of D_{cj} and P_{cj} using the shock jump conditions and the sonic condition for the CJ state. Consequently, P_{cj} can be determined from the particle velocity of the shock in the window to first order in Δu, or to second order in Δu with data from 2 experiments with different windows.

4 Summary

Simulations have been run to investigate the approach of a planar detonation wave to the steady CJ detonation for two explosives. The first is the TATB based PBX 9502 using the SURFplus model with a fast hotspot reaction and a second slow reaction for the energy released by carbon clustering. The second is the HMX based PBX 9501 using the SURF model with just a fast hotspot reaction. A detonation wave for both simulations was promptly initiated with a 1 mm hotspot consisting of the products at the CJ state.

For PBX 9502, at initiation the carbon clustering reaction progress variable is small and the detonation speed and VN spike pressure are a few per cent below the values for a CJ detonation. It takes about 100 mm of propagation for the detonation to be sufficiently close to steady state such that the CJ state can be readily identified from a sequence of pressure profiles in time.

In contrast, for PBX 9501 the detonation wave at initiation slightly overshots the CJ detonation speed and VN spike pressure. But within a 1 μs the steady CJ detonation wave is reached.

A consequence of the long approach to steady state for PBX 9502 is that it would be difficult for an experiment to maintain a planar detonation for sufficiently long to accurately measure the CJ pressure. Even for PBX 9501, a reaction zone profile experiment in which a detonation wave impacts a window and the interface particle velocity is measured with a PDV probe, it would be difficult to account for impedance mismatch with the window to accurately determine the CJ pressure. Such experiments would be suited to use as a model validation test.

References

J. B. Bdzil and W. C. Davis. Time-dependent detonations. Technical Report LA-5926-MS, Los Alamos National Lab., 1975. URL https://permalink.lanl.gov/object/tr?what=info:lanl-repo/lareport/LA-05926-MS. 4, 15

R. E. Duff and E. Houston. Measurement of the Chapman-Jouguet pressure and reaction zone length in a detonating high explosive. *J. Chem. Phys.*, 23:1268–1273, 1955. URL https://doi.org/10.1063/1.174255. 15

R. L. Gustavsen, S. A. Sheffield, and R. R. Alcon. Progress in measuring detonation wave profiles in PBX 9501. In *Eleventh (International) Symposium on Detonation*, pages 821–827, 1998. 14

R. L. Gustavsen, B. D. Bartram, and N. J. Sanchez. Detonation wave profiles measured in plastic bonded explosives using 1550 nm photon Doppler velocimetry. In *AIP Conference Proceedings 1995, 253*, 2009. URL https://doi.org/10.1063/1.3295117. 2

R. Menikoff. Effect of resolution on propagating detonation wave. Technical Report LA-UR-14-25140, Los Alamos National Laboratory, 2014. URL https://dx.doi.org/10.2172/1136940. 12

R. Menikoff. Detonation wave profile. Technical Report LA-UR-15-29498, Los Alamos National Lab., 2015. URL https://doi.org/10.2172/1229720. 4

R. Menikoff. Shock detector for SURF model. Technical Report LA-UR-16-20116, Los Alamos National Lab., 2016. URL https://doi.org/10.2172/1234496. 2

R. Menikoff. SURFplus model calibration strategy. Technical Report LA-UR-17-22073, Los Alamos National Lab., 2017. URL https://doi.org/10.2172/1346849. 2, 12

R. Menikoff and M. S. Shaw. Reactive burn models and Ignition & Growth concept. *EPJ Web of Conferences*, 10, 2010. URL https://dx.doi.org/10.1051/epjconf/20101000003. 2

R. Menikoff and M. S. Shaw. The SURF model and the curvature effect for PBX 9502. *Combustion Theory And Modelling*, pages 1140–1169, 2012. URL https://dx.doi.org/10.1080/13647830.2012.713994. 2

M. S. Shaw and J. D. Johnson. Carbon clustering in detonations. *J. Appl. Phys.*, 62:2080–2085, 1987. URL https://doi.org/10.1063%2F1.339554. 2